Non-linear shape approximation via the entropy scale space

Benjamin B. Kimia
Brown University
Providence, RI 02912
kimia@lems.brown.edu

Allen R. Tannenbaum
University of Minnesota
Minneapolis, MN 55455
tannenba@ee.umn.edu

Steven W. Zucker
McGill University
Montreal, Qc, Canada
zucker@mcrcim.mcgill.edu

ABSTRACT

There are two classical approaches to approximating the shape of objects. The first is based on diffusion and often leads to the (Gaussian) smoothing of contour information. The resulting scale-space may often be viewed as generated by parabolic operators which progressively and globally smooth shapes. The second approach is based on morphological morphology operations which represent the interior of shapes as sets, *e.g.*, a collection of disks. The resulting morphological space can be viewed as being defined via a hyperbolic operator whose weak or viscosity solutions progressively smooth shapes in a local manner. We are developing a general theory of shape which unifies these two different approaches in the *entropy scale space*. The theory is organized around two basic intuitions: first, if a boundary were changed only slightly, then, in general, its shape would change only slightly. This leads us to propose an operational theory of shape based on incremental contour deformations. The second intuition is that not all contours are shapes, but rather only those that can enclose "physical" material. A novel theory of contour deformation is derived from these intuitions, based on abstract conservation principles and the Hamilton-Jacobi theory. The result is a characterization of the computational elements of shape: protrusions, parts, bends, and seeds (which show where to place the components of a shape); and leads to a space of shapes (the reaction-diffusion space) which places shapes within a neighborhood of "similar" ones. Previously, these elements of shape have been used for description. We now show how they can be used to generate another space for shapes, the *entropy scale space*, which is obtained from the reaction-diffusion space by running the "reaction" portion of the equations "backwards" in time. As a result distinct components of a shape can be removed by introducing a minimal disturbance to the remainder of the shape. For example, imagine an image of don Quixote holding a lance. Within the entropy scale space the lance can be removed without disturbing the shape of his body. In contrast, if Gaussian smoothing techniques were used, the extent of the lance would effect the amount of distortion introduced to the rest of his body. As such, the entropy scale space is a combination of smoothing due to shocks as "black holes" of information and the subsequent rarefaction wave reconstruction, and the anisotropic diffusion process spreading of contour information. Our technique is numerically stable, and several examples will be shown.

1. INTRODUCTION

Visual structure is naturally perceived in a hierarchy of different scales, and as such, a qualitative understanding of an image should reflect these different scales. To cite the classical example, fingers exhibit structure at a finer scale than hands, hands are finer than limbs, and so on. Thus there is a connection between scale and size, and, for many applications in computer vision, scale size became synonymous with operator size. Big operators select structure at large scales, and small operators select structure at fine scales; one need only recall the tree image in [33] to recall the force of this argument; see also [39, 33, 26, 50] as well as the psychophysical support they were engaging [8, 47]. A scale-based representation is necessary not only to build a taxonomy of features, but also to deal with changes in resolution [25, 27], to match from coarse to fine, and to effectively communicate images [7].

But confounding these assessments of structure is noise, which suggests a different interpretation of operator size: big operators smooth large fractions of the image, while small operators smooth only tiny fractions. This confounding is clear for the "hand" above, in respect of which the "fingers" are just noise. Witkin [48] put these two interpretations together by suggesting a continuum of operators in a kind of *scale space*. Structure was captured by signal extrema, and these were computed not over a few neighborhood sizes, but over a *continuum* of neighborhoods, established by convolution against Gaussians of increasing extents. The behavior of extrema as the signal is smoothed out yields the qualitative description of the signal. In addition, a hidden bonus emerged in the form of a significance hierarchy on the extrema, in the sense that the extrema that survive larger smoothing extents are considered more significant. This is analogous to

 0-8194-1280-5/93/$6.00

	Signal	Feature	Process
Witkin	Intensity	Zero-crossings in Derivatives	Gaussian Smoothing
Mokhtarian & Mackworth	Boundary Coordinates	Inflection Points	Gaussian Smoothing
Richards et. al.	Boundary Orientation	Curvature Extrema	Gaussian Smoothing
Asada & Brady	Boundary Curvature	Extrema & Inflection Points	Gaussian Smoothing
Koenderink	Interior Chracteristic Function	Inflection Points	Gaussian Smoothing + Thesholding
Pizer et. al.	Interior Chracteristic Function	Symmetric Axis	Gaussian Smoothing + Normalized Thesholding

Figure 1: This figure reviews some of the proposed scale spaces. Note that the use of Gaussian smoothing is prominent.

the fingers being smoothed out before the hand. The space of the signal and its continuously smoothed versions is the *scale space* for the signal.

1.1. Parabolic Diffusion and Gaussian Smoothing

The question thus arises of how to "smooth" the signal so that only increasingly "significant" features survive further smoothing. Koenderink showed that, given assumptions of *causality, homogeneity, and isotropy*, the diffusion equation is the only sensible way of embedding a signal in a family of simpler signals with the requirement that structure is not created [25, 27]. From a different perspective, Babaud *et al.*independently showed that the Gaussian is the unique smoothing kernel that does not create structure in that with increased smoothing no new zero-crossings are created [6]. Yuille and Poggio extended this result to two dimensions [49] and Hummel and Monoit showed that zero-crossings, when supplemented with gradient data along the zero-crossing boundaries, are sufficient to reconstruct the original signal.

While these theorems and the popularity of Gaussian scale-spaces attest to its functionality in certain domains, Figure 1, it does not always provide "semantically meaningful" descriptions of images [37]. Rather, the above notions of structure are often not the natural ones, and Gaussian scale spaces may lead to more problems than they solve. For example, in an edge-detection Gaussian scale-space the true location of edges is not available. Instead, the true location is estimated by tracking edges across the scale space. Furthermore, the edges, which are very high in information content, become blurred out in the Gaussian representation. This point is illustrated even more powerfully in the domain of shape, and exemplified by the depiction of "don Quixote" in Figure 2. Ideally a scale-space representation of this profile should relate the structure of "the man on the horse with a lance" to that of "the man on the horse". Unfortunately, in the Gaussian scale-space representation of the shape, the lance assumes a role much more significant than it has in the original image. In fact, the longer the lance is, the more it dominates and distorts the remainder of the shape [1].

Thus, for Gaussian scale spaces, the "cure" almost seems worse than the "problem"; once the lance has been blurred together with don Quixote, it is almost impossible to remove it. Now, the situation is starting to look rather bleak, since the uniqueness theorems would seem to exclude other smoothing options for building scale-spaces. However, these theorems in fact make strong smoothness assumptions and do not hold when the scale space is extended to include non-differentiable or even non-continuous signals. Perona and Malik relax the homogeneity assumption and suggest that the candidate paradigm for generating a multiscale description should satisfy *causality, immediate localization,* and *piecewise smoothing* [37]. As before, causality requires that spurious detail should not be generated while passing from coarse to fine; immediate localization requires sharp scale-invariant placement of boundaries; and piecewise smoothing encourages intraregion over interregion smoothing. To alleviate the latter problem, they suggest that diffusion be location dependent, or anisotropic, for edge-detection.

1.2. Morphological Filters

Other approaches such as mathematical morphology argue that much stronger nonlinearities are necessary. Mathematical morphology views binary images as sets and grayscale images as functions or topographic reliefs. These sets and functions

[1] See [6] for an illustration of the "dumbbell" problem.

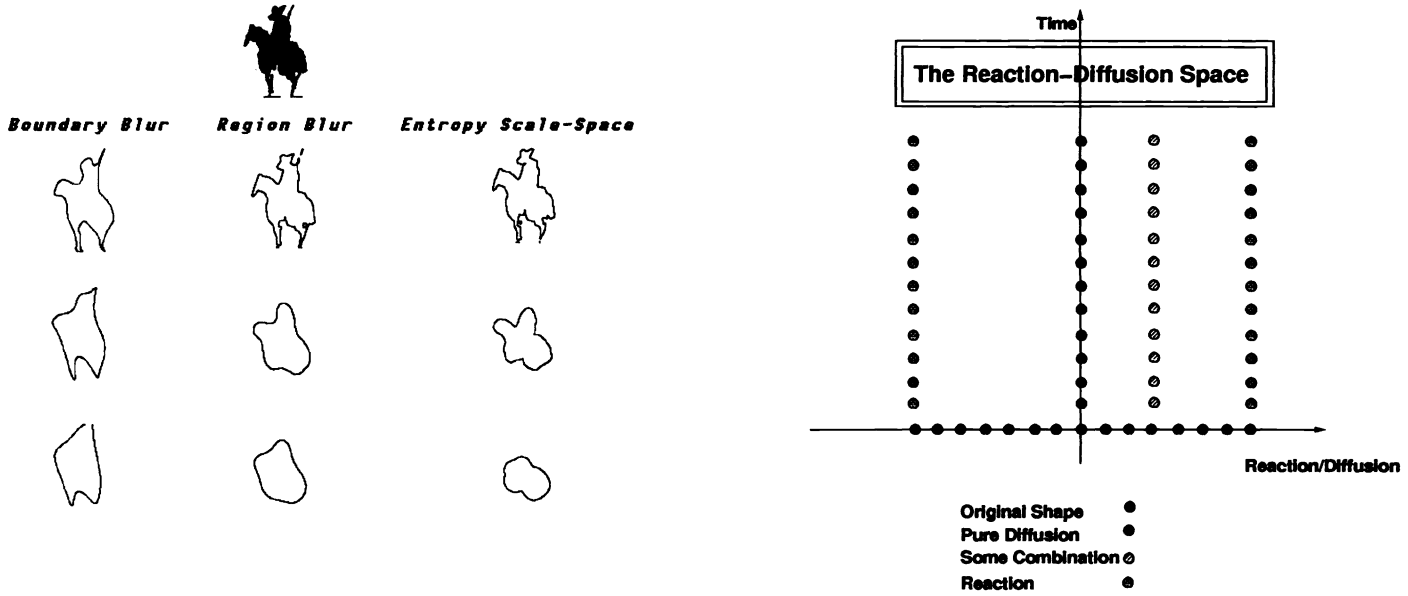

Figure 2: Left) A depiction of don Quioxte. The left column illustrates three instances of the process of blurring the boundary coordinates; the middle column displays effects of blurring the characteristic function of the interior of the shape. On the right, three steps along one axis of the entropy scale-space is shown. Note, that while the lance as well as other features of the shape are distributed throughout the shape by Gaussian smoothing, this does not happen in the entropy scale-space. Here, small features like the lance are removed without affecting the larger structures. Right) The reaction-diffusion space represents a range of deformations: diffusion corresponds to deformations by curvature motion alone, while reaction is deformations by constant motion (both in and out) along the normal. Intermediate points are combinations of the two deformations. Time is the amount of deformation in all cases.

are then transformed—in the spatial domain—via *morphological transformations,* whose definitions are usually based on *structuring elements, i.e.*, particular shapes that are translated in the images and used as probes. Morphological transformations can be built in an incremental way starting from the simplest ones, *erosions* and *dilations* [43, 44, 15]. The erosion of a set X is defined as the the locus of the positions of the center of the structuring element when it is translated over the set X and it is completely included in it. From erosion and dilation operations one derives the classic *openings* and *closings* operations as well as morphological gradients, granulometries and hit-or-miss transformations, leading to skeletons and watersheds. The mathematical morphology approach represents the notion of scale by operators of increasing sizes, leading to morphological scale spaces [31, 10, 32]. Chen and Yan showed that the morphological opening filter does not introduce new zero-crossings as one moves to coarser scales; see also [32].

The classical set theoretic, algebraic view of mathematical morphology is complemented by a geometric, differential view when the morphological operations are considered as steps in a differential deformation of the shape [21, 5]. It was shown that mathematical morphology operations with a convex structuring element are captured by a differential deformation of the boundary along the normal, governed by a Hamilton-Jacobi partial differential equation [5].

We will explore this geometric connection later in the paper to bridge the immense conceptual transition from parabolic diffusion such as Gaussian smoothing to mathematical morphology; somehow, to be generally applicable, scale spaces must be extended to include these extremes. Our goal in this paper is to propose a formal mathematical framework for abstraction of information in a signal in which parabolic diffusion and morphological operations are special cases.

2. A FRAMEWORK FOR REPRESENTING SHAPE

2.1. Shape from deformation

Entropy scale-space evolved from our framework for representing shape. One of the basic axioms in this framework is that slightly deformed shapes appear similar to the original shape. To establish this connection, we studied the deformation of closed curves under arbitrary deformations [22].

$$\mathcal{C}_t = \beta(s,t)\vec{N}, \tag{1}$$

where C is the curve, t is time (or the amount of deformation), s is the parameter along the curve (not necessarily the arclength), $\vec{N}$ is the normal. Intriguingly, arbitrary intrinsic deformations can be classified into a) constant motion along the normal to the boundary of the curve,*constant motion*, and b) motion along the boundary with magnitude proportional to the curvature of the curve at that point, *curvature motion*. These two basis of deformations have complementary properties and capture various properties of shape along the axes of linear/nonlinear, local/global and boundary/region. Formally,

$$C_t = (\beta_0 - \beta_1 \kappa)\vec{N}, \tag{2}$$

where κ is curvature, and β_0, β_1 determine the combination of constant and curvature motions [2]. For mathematical, as well as numerical, reasons the problem of curve evolution is cast as a higher-dimensional, surface evolution problem [18, 23] with the property that the zero-level set evolves according to equation (2). Let the surface be defined by $z = \phi(x, y, t)$ such that its zero levet set $\phi(x, y, t) = 0$ is exactly the trace of the curve $C(s, t) = (x(s, t), y(s, t))$. Thus, we have $\phi_t + \beta(\kappa)|\nabla\phi| = 0$, or when $\beta(\kappa) = \beta_0 - \beta_1\kappa$,

$$\phi_t + \beta_0|\nabla\phi| = \beta_1[-\frac{(\phi_{xx}\phi_y^2 - 2\phi_{xy}\phi_x\phi_y + \phi_{yy}\phi_x^2)}{(\phi_x^2 + \phi_y^2)^{3/2}}]. \tag{3}$$

2.2. The role of conservation laws

It is interesting that constant motion leads to a hyperbolic conservation law for the orientation of the curve [19, 20, 18]:

Theorem 1 *Orientation of a curve deformed by constant motion satisfies*

$$\frac{\partial\theta}{\partial t} + \mathcal{H}_\theta(\theta)_x = 0, \tag{4}$$

where $\mathcal{H}_\theta(\theta) = \cos(\theta)$, $-\pi/2 < \theta \leq \pi/2$; clearly a hyperbolic conservation law for orientation θ.

Curvature motion, on the other hand, adds viscosity to the system:

Theorem 2 *Orientation of a curve deformed by a combination of constant motion and curvature motion satisfies*

$$\theta_t + \beta_0[\mathcal{H}(\theta)]_x = \beta_1 \cos^2(\theta)\theta_{xx}, \tag{5}$$

where $\mathcal{H}_\theta(\theta) = \cos(\theta)$, namely a viscous hyperbolic conservation law for orientation θ.

Since conservation laws are nonlinear, initially smooth functions often lead to singularities, or *shocks*. The formation and classification of these shocks is governed by a notion of *entropy*. The interaction of these shocks is key to understanding shape. As such, we define the space of all combinations of constant and curvature deformations for all times as the *reaction-diffusion* space, Figure 2. Formally, the reaction-diffusion space for a shape $\mathcal{S}$ is the set of all shapes $\mathcal{S}'$ generates by

$$\mathcal{RD}_{(\alpha,t)} : \mathcal{S} \longrightarrow \mathcal{S}', \tag{6}$$

where $\mathcal{RD}$ is the deformation with α as the ratio of constant motion to curvature motion magnitudes and t is time.

2.3. Shape deformations and smoothing

What is particularly interesting is the connection between pure curvature motion and Gaussian smoothing [18]:

Theorem 3 *Consider the family of curves $C(s,t)$=$(x(s,t), y(s,t))$ satisfying*

$$\begin{cases} \frac{\partial C}{\partial t} & = -\kappa(s,t)\vec{N} \\ C(s,0) & = C_0(s), \end{cases} \tag{7}$$

where $C_0(s) = (x_0(s), y_0(s)$ is the initial curve, s is some arbitrary parameter along the curve, t is time, κ is curvature, and $\vec{N}$ is the normal. Then the coordinates satisfy the diffusion equation

$$\begin{cases} \frac{\partial x}{\partial t} = \frac{\partial^2 x}{\partial \tilde{s}^2} & x(\tilde{s}, 0) = x_0(\tilde{s}) \\ \frac{\partial y}{\partial t} = \frac{\partial^2 y}{\partial \tilde{s}^2} & y(\tilde{s}, 0) = y_0(\tilde{s}), \end{cases} \tag{8}$$

where $\tilde{s}$ is the arclength parameter along the curve.

[2] The sign of β_1 is negative to stress that running curvature motion backward in time is equivalent to running the heat equation backwards in time which is ill-conditioned.

In other words, locally, curvature motion smooths the boundary coordinates by the diffusion (heat) equation whose kernel is the Gaussian [46]. Note that since arclength parameterization is not preserved in the smoothing process, smoothing by curvature motion is a nonlinear analogue of Gaussian smoothing as used in [35].

A strong connection exists between the classic heat equation [27], anisotropic diffusion [37, 9, 1] and evolution by curvature [24], namely when $\beta(\kappa) = -\kappa$. The latter equation is represented by the following surface evolution

$$\phi_t = \kappa|\nabla\phi|, \tag{9}$$

which may be rewritten as

$$\phi_t = |\nabla\phi| div(\frac{\nabla\phi}{|\nabla\phi|}). \tag{10}$$

On the other hand, the classical heat equation is

$$\phi_t = \Delta\phi. \tag{11}$$

When the component of the diffusion across each edge, namely along the gradient, is subtracted, we have

$$\phi_t = \Delta\phi - \frac{1}{\|\nabla\phi\|^2}\langle\nabla^2\phi(\nabla\phi), \nabla\phi\rangle, \tag{12}$$

where $\nabla^2\phi$ denotes the Hessian of ∇. It is not difficult to show that this is equivalent to equation (9), thereby demonstrating the surprising connection that deformation by curvature of each level set of an intensity image is tantamount to anisotropic diffusion.

The other of our basis deformations, constant motion, operates in a complementary fashion. To describe this process, we first illustrate the process of shock formation and the role of entropy which allows us to view shocks as "black holes of information".

2.4. Formation of Shocks and Entropy

Conservation laws appear frequently in physical sciences. Examples include conservation of matter, energy, electric charge, heat, among others. To illustrate, consider conservation of matter: "the amount of matter that flows into a volume is exactly the amount of increase of matter within that volume". In other words, "matter is neither created nor destroyed". Consider a single hyperbolic conservation law,

$$\begin{cases} u_t + [f(u)]_x &= 0, \\ u(x,0) &= u_0(x), \end{cases} \tag{13}$$

where u is the conserved quantity, t is time, x is the spatial coordinate, and f is the flux [29]. This is often a nonlinear equation which will frequently lead to singularities, even if the initial data is smooth. As such, the usual space of differentiable, or even continuous function no longer captures the physical solutions beyond the development of the singularity. One possibility is to enlarge the space to one of *generalized functions*. Unfortunately, there are too many solutions satisfying the above partial differential equation with the initial condition. Since the physics of the solution determines a single function, the question arises as how to determine the physically significant solution. The answer lies in the notion of *entropy* [28, 36], to pick the physical vsicosity solution [11], and which in the case of gas dynamics reduces to "entropy of the particles must increase as they cross a *shock* front".

To illustrate the notions of shock and entropy, let us consider the *characteristics* of equation (13),

$$\frac{dx}{dt} = \frac{df}{du}. \tag{14}$$

To recall, characteristics are trajectories in the (x,t), or space and time domain, over which u remains constant. Consider then, a well-studied example of a hyperbolic conservation law, the Burgers' equation [16], where $f(u) = \frac{1}{2}u^2$, leading to $dx/dt = u$. Given initial condition

$$u_0(x) = \begin{cases} 1 & \text{if } x \leq 0 \\ 1-x & \text{if } 0 \leq x \leq 1 \\ 0 & \text{if } 1 \leq x, \end{cases} \tag{15}$$

all points on the negative x-axis will move to the right with speed 1, all points with $x \geq 1$ stay put, while all points with $0 \leq x < 1$ will move to the right with intermediate speeds. It is clear from Figure 3 that for $t < 1$ the function $u(x,t)$

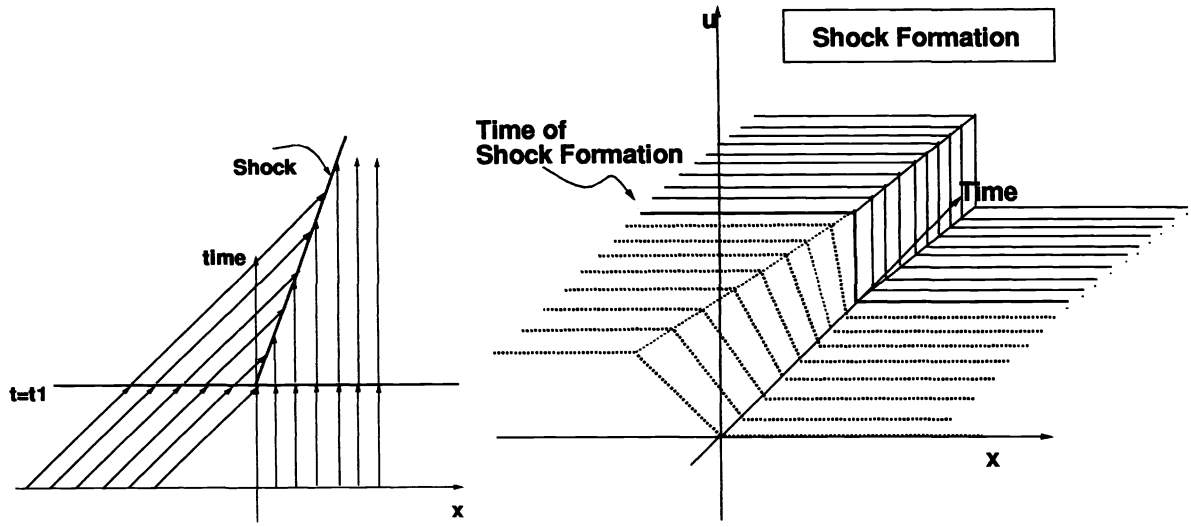

Figure 3: This figures illustrates how characteristics clash and shocks form. Note that after the shock forms, it travels as a shock. Therefore, singularities are explicitly represented in the context of generalized functions.

remains single valued. However, for $t \geq 1$, the characteristics clash, and there exists the potential for the formation of a *shock*. At this point, the two characteristics enforce two different values for u, which is clearly not possible. The dilemma of which of the two values is physically meaningful is solved by enforcing conservation at the shock, leading to the so-called *jump condition* [3]

$$s(u_r - u_l) = f_r - f_l, \tag{16}$$

where l and r denote left and right, respectively, and s is the speed with which the shock will move. For the case of Burgers' flux, the shock will move with the average speed of the two incoming characteristics.

A second problem arises when we consider diverging characteristics. Consider the initial condition

$$u_0(x) = \begin{cases} 0 & \text{if } x < 0 \\ 1 & \text{if } 0 < x \end{cases} \tag{17}$$

where there will be points whose value can not be determined as is depicted in Figure 4. The gap may be filled using the jump condition, however we find that many solutions exists in conjunction. The entropy condition rules out the above example as a possible discontinuous solution by imposing that characteristics always flow into the discontinuity [28, 36, 45] A discontinuity satisfying both the jump condition and the entropy condition is called a *shock*. The important theorem is provided by Lax, who shows that a generalized solution of equation (13) which has only shocks as discontinuities exists and is unique [29].

2.5. Shocks as Black Holes of Information

The key to the connection between scale-space and hyperbolic conservation laws is a view of shocks as "black holes of information" [18]. To qualify, let us consider equation (13) and the initial condition (15). Up to the time of shock formation the process is reversible in that the signal may be recovered by tracing the characteristics back in time. As such the information content of the signal remains the same up to the formation of a shock. However, at any point past shock formation, the process is irreversible. In fact, in the context of gas dynamics this irreversibility and that entropy must increase across a shock (and therefore loss of information) has long been recognized [45, 30]. Any attempt in the recovery of the initial signal will be successful only for those characteristics that can be traced back in time, that is any point other than the shock itself. However, the shock point maps to a region of the initial signal, namely, its *domain of dependence* [12]. Therefore, information contained in this section of the signal is irreversibly lost, Figure 4. It is with this view that we have termed a shock a "black hole" of information: with increasing time, increasingly larger sections of the

[3] Also known as the Rankine-Hugoniot condition.

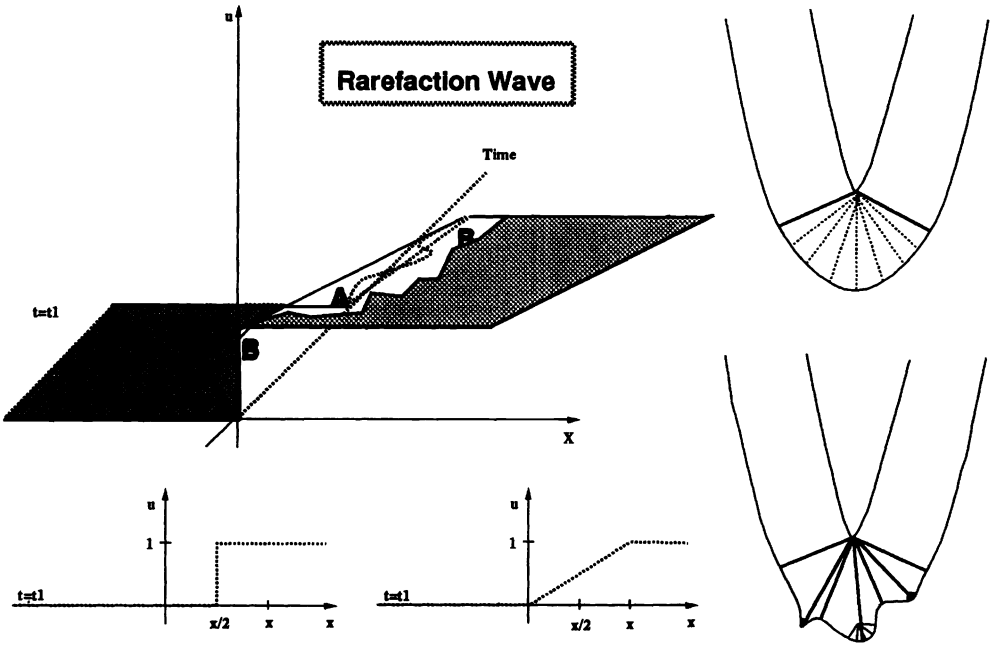

Figure 4: This figures illustrates a rarefaction wave and how it relates to the idea of a shock as a "black hole of information". (Left) The initial condition represents a shock from which characteristics diverge to produce a gap between determined values. How should the function continue in time (the two graphs represents two possibilities)? The entropy condition determines the outcome here which in the case of the conservation law for shape corresponds to a circular reconstruction centered at the shock. (Top Right) This figures illustrates how a convex figure deforms in time form a shock. Once a shock is formed, the information contained in the section of the curve which mapped to the shock in the forward direction (between dashed lines) is now lost forever. Note that the removal of information is local, and nonlinear. An attempt to reconstruct the original signal yields a circular arc for the section that maps to the shock. (Bottom Right) This is an illustration of the hierarchy imposed by shocks: less significant shocks corresponding to protrusions get absorbed in larger shocks describing the more global shape of the object. Again the back reconstruction gives the same circular arc, even though the section mapping to the shock is now more complicated.

signal map onto the shock, irrevocably lost. Other sections of the signal, however, can be recovered fully and exactly. This is, therefore, a local process whose domain increases with time and eventually becomes global.

An interesting question is what happens to the lost section of the signal upon recovery. The non-shocks points can be retrieved by running the *same* process backwards in time [4]. However, the process of running a shock backwards in time, leads to a rarefaction wave which generates a continuous solution connecting the two disparate ends while satisfying conservation. For the case of shape and conservation of orientation this will be equivalent to arc of circle approximation.

Remark. The preceding theory of curve evolution is Euclidean invariant. Very recently, an affine invariant approach has been developed in [41, 42, 40], where it is shown that the unique affine invariant evolution is

$$\frac{\partial \mathcal{C}}{\partial t} = \kappa^{1/3} \vec{N}. \tag{18}$$

This evolution has a number of remarkable properties, for example, it shrinks the affine perimeter as quickly as possible, and converges to an ellipse.

3. The Entropy Scale Space

The key motivation behind the entropy scale space is to combine two complementary approaches to smoothing shape in a unified framework: global parabolic diffusion smoothing methods, on the one hand, and local smoothing and shock generating filters such as morphological operators, on the other. Our framework for shape begins with simple intuitive

[4] For the diffusive-type conservation laws (e.g. heat equation) this process is ill-conditioned, however for the wave-type (e.g. our case), this process has proven extremely robust.

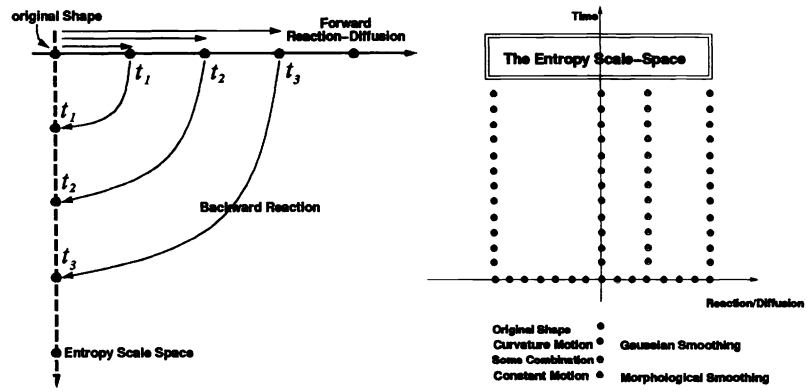

Figure 5: Left) This figure illustrates the process of constructing the entropy scale space. A point $(\beta 0, \beta 1, t)$ of the entropy scale space is the result of the reaction-diffusion process at $(\beta 0, \beta 1, t)$ and a subsequent process $(-\beta 0, 0, t)$. Informally, run reaction-diffusion forward in time and then run reaction backward in time. The time corresponding to each pair of deformations together with the ratio of reaction to diffusion spans the entropy scale space. Right) A depiction of the entropy scale space.

axioms and leads to the *reaction-diffusion space* where the shape is deformed in various ways and a description is obtained via the formation of shocks. We now show how to use this description to approximate shapes in the *entropy scale space* whose extremes define the above approaches.

Informally, parabolic diffusion, such as Gaussian smoothing, smooths shapes by globally propagating information. Information is thus lost globally at each finite resolution. On the other hand, morphological operators annihilate information locally by selectively removing parts of the shape, while leaving others unaffected. The entropy scale space captures the first kind of smoothing via *curvature deformation* which gives rise to a parabolic diffusion equation as was shown in Theorem 3. The second kind of operation is captured by a pair of *constant deformations,* and can best be explained in terms of shock formations and rarefaction waves. In the process of the first constant deformation shocks form which remove information locally. This information is lost forever. Indeed, attempting to reverse the course of time produces a rarefaction wave. In other words, the first constant deformation produces shocks and the second constant deformation (in the opposite direction) reconstructs what is possible through the rarefaction wave. Given the flux of conservation law (4), the rarefaction wave effectively replaces pieces of the boundary of the shape with a circular reconstruction. Thus, these two evolutions capture the basic diffusion and morphological processes of interest in image analysis and shape approximation; see Figure 5.

Formally, the *entropy scale space* is the set of all shapes $\mathcal{S}''$ generated from $\mathcal{S}$ by first deforming the shape by some combination of constant and curvature motion magnitudes, (β_0, β_1), for time $T/2$ to get $\mathcal{C}_1(s)$,

$$\begin{cases} \frac{\partial \mathcal{C}}{\partial t} & = (\beta_0 - \beta_1 \kappa)\vec{N} \\ \mathcal{C}(s,0) & = \mathcal{C}_0(s). \end{cases} \tag{19}$$

and then deforming $\mathcal{C}_1(s)$ by a related combination of constant and curvature motion magnitudes, $(-\beta_0, 0)$, for time $T/2$ to get $\mathcal{C}_2(s)$,

$$\begin{cases} \frac{\partial \mathcal{C}}{\partial t} & = -\beta_0 \vec{N} \\ \mathcal{C}(s,0) & = \mathcal{C}_1(s). \end{cases} \tag{20}$$

which gives the boundary of $\mathcal{S}''$, Figure 6. It should be noted that in fact these equations are implemented by considering the curves as level curves on a corresponding deforming family of surfaces, equation (3). This allows us an explicit treatment of shocks using viscosity theory.

Alternatively, we may write this process as a single PDE; consider the solution $\hat{\mathcal{C}}(s, \tau, t)$ of the following PDE:

$$\begin{cases} \frac{\partial \hat{\mathcal{C}}}{\partial \tau} & = \chi_{(0,t/2)}(\tau)(\beta_0 - \beta_1 \kappa)\vec{N} + \chi_{(t/2,t)}(\tau)(-\beta_0)\vec{N} \\ \hat{\mathcal{C}}(s,0) & = \mathcal{C}_0(s), \end{cases} \tag{21}$$

where $\chi_S(t)$ is the characteristic function of the set S. Then, pick $\mathcal{C}(s,t) = \hat{\mathcal{C}}(s,t,t)$. In practice, first the reaction-diffusion space for a shape is computed and the resulting shapes are then run backward to construct the entropy scale space, Figure 5.

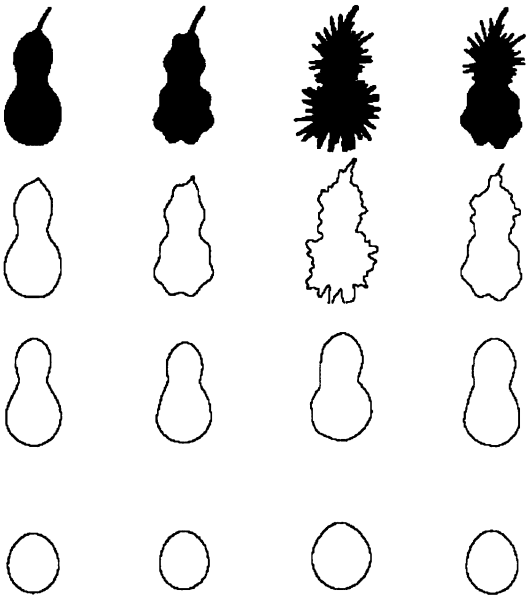

Figure 6: Samples from a slice through the entropy scale-space are displayed for four pears. Note that the similarity that emerges with increased smoothing provides a basis for building a similarity measure between shapes for object recognition.

Why should this process approximate a signal or a shape? Let us first examine the effect of curvature motion along the normal which like Gaussian smoothing propagates information *globally* and instantaneously. Through this propagation smaller features amalgamate with larger ones so that subsequent quantizing of the signal removes small-scale information altogether [17]. Grayson showed that all embedded curves evolving by curvature converge to a circular point without developing self-intersections [13, 14]. We have also shown that curvature motion, or the so-called *geometric heat equation* defines an anisotropic diffusion in the sense of Perona and Malik, equation (9). This process satisfies the criterion that structure is not created in this process and it is indeed one which leads towards simplifying the signal. The smoothing, however, is based on the boundary of the object where a feature with larger length is more significant (recall the lance of don Quixote) which is not always desirable. Rather, in addition to these *boundary* considerations, scale should also include *region* based concepts. Furthermore, this process smooths all singularities indiscriminately.

In contrast, the process of the entropy scale space when only constant motion is used acts locally on the signal so that while parts of it are simplified, others remain intact. It brings together points which are remote along the boundary but are close in space though the interior *region*. This process is exactly equivalent to the morphological operations of opening and closing (closure) with a circular [5] structuring element through an application of Hüygens principle. Furthermore, some singularities are preserved even as the shape is being simplified. We now show several results which formalize this.

3.1. On the properties of the Entropy scale space

A number of formal measures are now introduced to show that the entropy scale space does indeed lead to simplification of the shape without creation of new structure. Specifically, we show that the *total absolute curvature* is nonincreasing, and no new *zeros* of curvature, *minima*, or *maxima* of curvature may be created.

3.1.1. Total absolute curvature

While viewed as a curve, as scale increases the shape becomes simpler in the sense that the total absolute curvature is nonincreasing [22].

Theorem 4 *Let $C(s,t)$ be a solution of*

$$\begin{aligned} \frac{\partial \mathcal{C}}{\partial t} &= \beta(\kappa(s,t))\vec{N} \\ \mathcal{C}(s,0) &= \mathcal{C}_0(s), \end{aligned}$$

$t \in [0,t')$ and s some parameter along the curve $\mathcal{C}$. Suppose that $\kappa\beta(\kappa) \leq M$, and $\beta_\kappa \leq 0$ Then,

[5] See [5] for a generalization to all convex structuring elements.

$$\bar{\kappa}(t) \leq \bar{\kappa}(0),$$

where $\bar{\kappa}$ is the total absolute Gaussian curvature.

3.1.2. Extrema of Curvature

All the following results are simple corollaries of the following elegant theorem which itself is based on the maximum principle for parabolic operators [2, 3, 4, 34]: Let $u(x,t)$ be classical solution of the linear time-varying parabolic PDE,

$$u_t = a(x,t)u_{xx} + b(x,t)u_x + c(x,t)u, \tag{22}$$

on the rectangle $R_T := [x_o, x_1] \times [0,T]$, where the coefficients are assumed to be smooth, and $a(x,t)$ is positive. Suppose moreover that $u(x_i,t) \neq 0$ for $i = 0,1$, and $0 \leq t \leq T$. Let $z(t)$ be the number of zeros of $x \rightarrow u(x,t)$ counted with multiplicity. Then in [2, 34], it is proven that $z(t) < \infty$, and $z(t)$ is non-increasing function of t. Moreover, at any time t when $x \rightarrow u(x,t)$ has a zero of order $k > 1$, $z(t)$ drops by at least $k-1$.

To relate this to curves and the annihilation and creation of structure, let *vertices* denote points of maximal and minimal curvature,

$$\kappa_s(s,t) = 0, \quad \kappa_{ss}(s,t) \neq 0, \tag{23}$$

and *flexes* denote zero-crossings of curvature. Consider deformations of shape according to equation (2) where curvature evolves by [22],

$$\frac{\partial \kappa}{\partial t} = \beta_1 \kappa_{\tilde{s}\tilde{s}} + \beta_1 \kappa^3 - \beta_0 \kappa^2. \tag{24}$$

Consider a fixed t and assume that there are only a finite number of flexes and vertices. When $\beta_1 = 0$, we have $\kappa_t = -\beta_0 \kappa^2$ which is explicitly solved as

$$\kappa(s,t) = \frac{\kappa(s,0)}{1 + \beta_0 t \kappa(s,0)}. \tag{25}$$

In this case,

$$\kappa_s(s,t) = \frac{\kappa_s(s,0)}{(1 + t\kappa(s,0))^2}, \tag{26}$$

namely, the number of vertices do not change, as long as the curve remains smooth. More generally, differentiate equation (24) with respect to $\tilde{s}$,

$$(\kappa_t)_{\tilde{s}} = \beta_1 (\kappa_{\tilde{s}\tilde{s}})_{\tilde{s}} + 3\beta_1 \kappa^2 \kappa_{\tilde{s}} - 2\beta_0 \kappa \kappa_{\tilde{s}} \tag{27}$$

and using [22],

$$\frac{\partial}{\partial t}\frac{\partial}{\partial \tilde{s}} = (-\beta_0 + \beta_1 \kappa)\kappa \frac{\partial}{\partial s} + \frac{\partial}{\partial \tilde{s}}\frac{\partial}{\partial t}, \tag{28}$$

we get

$$(\kappa_{\tilde{s}})_t = \beta_1 (\kappa_{\tilde{s}})_{\tilde{s}\tilde{s}} + 4\beta_1 \kappa^2 \kappa_{\tilde{s}} - 3\beta_0 \kappa \kappa_{\tilde{s}}. \tag{29}$$

Set $v := \kappa_{\tilde{s}}$. Then we see that

$$v_t = \beta_1 v_{\tilde{s}\tilde{s}} + (4\beta_1 \kappa^2 - 3\beta_0 \kappa) v. \tag{30}$$

Assuming that $\beta_1 > 0$, we see from the above discussion on parabolic PDE's, that we have that the number of vertices is nonincreasing as long as a classical solution exists.

3.1.3. Zeros of Curvature

To show that the number of flexes is nonincreasing, the same sort of argument works (again assuming that $\beta_1 > 0$). Indeed, since κ satisfies the parabolic equation

$$\frac{\partial \kappa}{\partial t} = \beta_1 \kappa_{\tilde{s}\tilde{s}} + (\beta_1 \kappa^2 - \beta_0 \kappa)\kappa, \tag{31}$$

we can apply [2, 3, 4, 34], to conclude that the number of zeros of κ in non-increasing. Therefore, the number of flexes does not increase. For $\beta_1 = 0$, that the number of flexes remains the same can be inferred directly from equation (25).

3.1.4. Self-intersections

To show that the number of self-intersections cannot increase, we express smooth portions of $\mathcal{C}_t$ as the graph of a function, *i.e.*,

$$y = u(x,t). \tag{32}$$

Note that in this case

$$\begin{aligned} \frac{\partial u}{\partial t} &= (1+u_x^2)^{\frac{1}{2}}(\beta_0 + \frac{\beta_1 u_{xx}}{\left(1+u_x^2\right)^{\frac{3}{2}}}) && (33)\\ &= G(u_x, u_{xx}) && (34)\\ & && (35) \end{aligned}$$

We need the following lemma:

Lemma 1 *Let $G(a,b)$ be a smooth function. Set*

$$\begin{aligned} G_1^*(a,b) &= \frac{\partial G}{\partial a}(a,b) && (36)\\ G_2^*(a,b) &= \frac{\partial G}{\partial b}(a,b), && (37) \end{aligned}$$

and assume that G_2^* is positive. Let u_1, u_2 be two solutions of

$$\frac{\partial u}{\partial t} = G(u_x, u_{xx}). \tag{38}$$

Then the number of zeros of $u_1(x,t) - u_2(x,t)$ is a non-increasing function of t.

Proof: First note that by the mean-value theorem

$$G(a,b) - G(c,d) = G_1^*(\zeta_1,\zeta_2)(a-c) + G_2^*(\zeta_1,\zeta_2)(b-d) \tag{39}$$

for (ζ_1,ζ_2) a point on the line connecting (a,b) and (c,d). Now for u_1, u_2 as above and $v = u_1 - u_2$, we therefore have by the mean-value theorem that

$$\begin{aligned} \frac{\partial v}{\partial t} &= G(u_{1x}, u_{1xx}) - G(u_{2x}, u_{2xx}) && (40)\\ &= G_1^*(\xi_1,\xi_2)(u_{1x}-u_{2x}) + G_2^*(\xi_1,\xi_2)(u_{1xx}-u_{2xx}) && (41)\\ &= G_1^*(\xi_1,\xi_2)v_x + G_2^*(\xi_1,\xi_2)v_{xx} && (42)\\ &= G_1(x,t)v_x + G_2(x,t)v_{xx} && (43) \end{aligned}$$

Once again, we get a linear parabolic PDE, and so the number of zeros of v does not increase. But the zeros of v are exactly points of intersection of u_1 and u_2. Note by [2, 34], the higher order zeros of v decrease. Hence, intersections with multiplicity greater than 1 are decreasing functions of time. □

3.1.5. Speed of shocks

Finally, we will be interested in trying to compute explicitly the shock paths. As a preliminary result, we would like to give the following fact about the speed of the shocks for curves evolving according to the Hüygens principle (prairie-fire model). Let

$$u(x,y,t) = 0, v(x,y,t) = 0$$

denote the equations of the evolved curves at time t. Then

$$\frac{\partial u}{\partial t} = |\nabla u| = \sqrt{u_x^2 + u_y^2},$$

$$\frac{\partial v}{\partial t} = |\nabla v| = \sqrt{v_x^2 + v_y^2}.$$

Now

$$\frac{du}{dt} = u_x \cdot \dot{x} + u_y \cdot \dot{y} + u_t = 0$$

$$\frac{dv}{dt} = v_x \cdot \dot{x} + v_y \cdot \dot{y} + v_t = 0$$

so that

$$\dot{x} = \frac{u_y v_t - v_y u_t}{u_x v_y - u_y v_x} = \frac{u_y |\nabla v| - v_y |\nabla u|}{u_x v_y - u_y v_x}$$

$$\dot{y} = \frac{v_x u_t - u_x v_t}{u_x v_y - u_y v_x} = \frac{v_x |\nabla u| - u_x |\nabla v|}{u_x v_y - u_y v_x}.$$

Thus we can conclude that the speed of the shock only depends on first order tangential information as explicitly given above. This gives a good initial guess of how the shock path is moving in the computation the shock path. Unfortunately, the path itself depends on all the derivatives.

4. EXAMPLES

We illustrate the entropy scale space for two simple shapes, the "icecream cone" and the "peanut" shapes, Figure 7, the don Quixote of Figure 2, Figure 8, and the four pears presented by Richards *et al.* [38], Figure 9. The pears sequence are interesting in that a normal shape (a normal "pear") is to be recognized when it is contaminated by various combinations of texture and noise.

To describe the figures, recall that the entropy scale space is a two dimensional space. One axis reflects relative amounts of reaction to diffusion, the other is time. We use logarithmic sampling of both axis [25]. There are no parameters so that tuning is not necessary. The diffusion extreme is parabolic, like Gaussian blurring, but smooths better. The reaction extreme on the other hand is equivalent to morphological operations of opening and closing (closure) with a ball structure element.

In these illustrations only inward constant deformations are used, thereby they depict the left portion of the entropy scale space. In particular, To compare the presentation of the pears in the entropy scale space, samples from a slice of each entropy scale space are displayed side-by-side, Figure 6. This figure demonstrates the potential for building a measure of similarity and a topology on shape, based on the entropy scale space. Note in particular that various features are smoothed out differently along the reaction and diffusion axes. This allows for a "space" rich enough to support a notion of metric whether the disparity between the original prototype and the image is boundary-based or region-based.

5. CONCLUSION

We have presented a general framework for representing scale. This framework is originally based on a representation for shape aimed at capturing similarity of slightly deformed shapes . These deformations satisfy a viscous conservation law and lead to the reaction-diffusion space in which shocks form and interact. Based on this space and the view of shock as a "black hole of information", we have built the entropy scale-space for approximating shape and signals. On the one hand, a slice through this space gives global parabolic anisotropic diffusion. On the other hand, another slice through this space is equivalent to the morphological operations of opening and closing, both nonlinear but local processes. Thus, in our framework these two different extremes combine to capture various aspects of the signal. It is indeed the combination of these smoothing methods, which contrast and complement each other, that is responsible for stable and robust results in an application of entropy scale-space to shape.

6. ACKNOWLEDGMENTS

Supported by grants from the National Science Foundation, the Natural Sciences and Engineering Research Council, the Air Force Office of Scientific Research, and by the Army Research Office. S.W.Z. is a Fellow of the Canadian Institute for Advanced Research. B.B.K. thanks Allan Dobbins and Lee Iverson for helpful discussions.

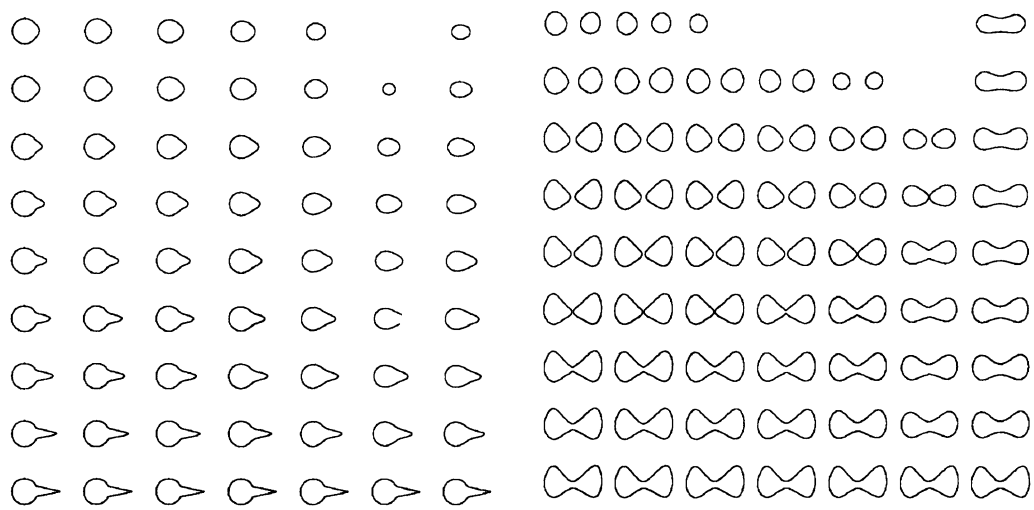

Figure 7: This figure represents the left half portion of entropy scale-space for the "icecream cone" and peanut shapes (128x128 binary images).

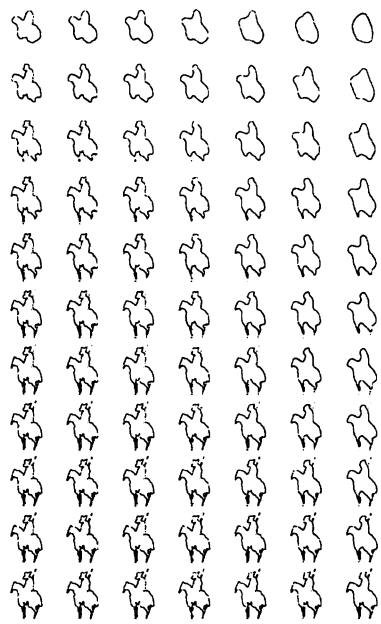

Figure 8: Don Quioxte in the left portion of the entropy scale space. Note the change in the method of smoothing when traversing the horizontal axis, in particular the significance of the lance.

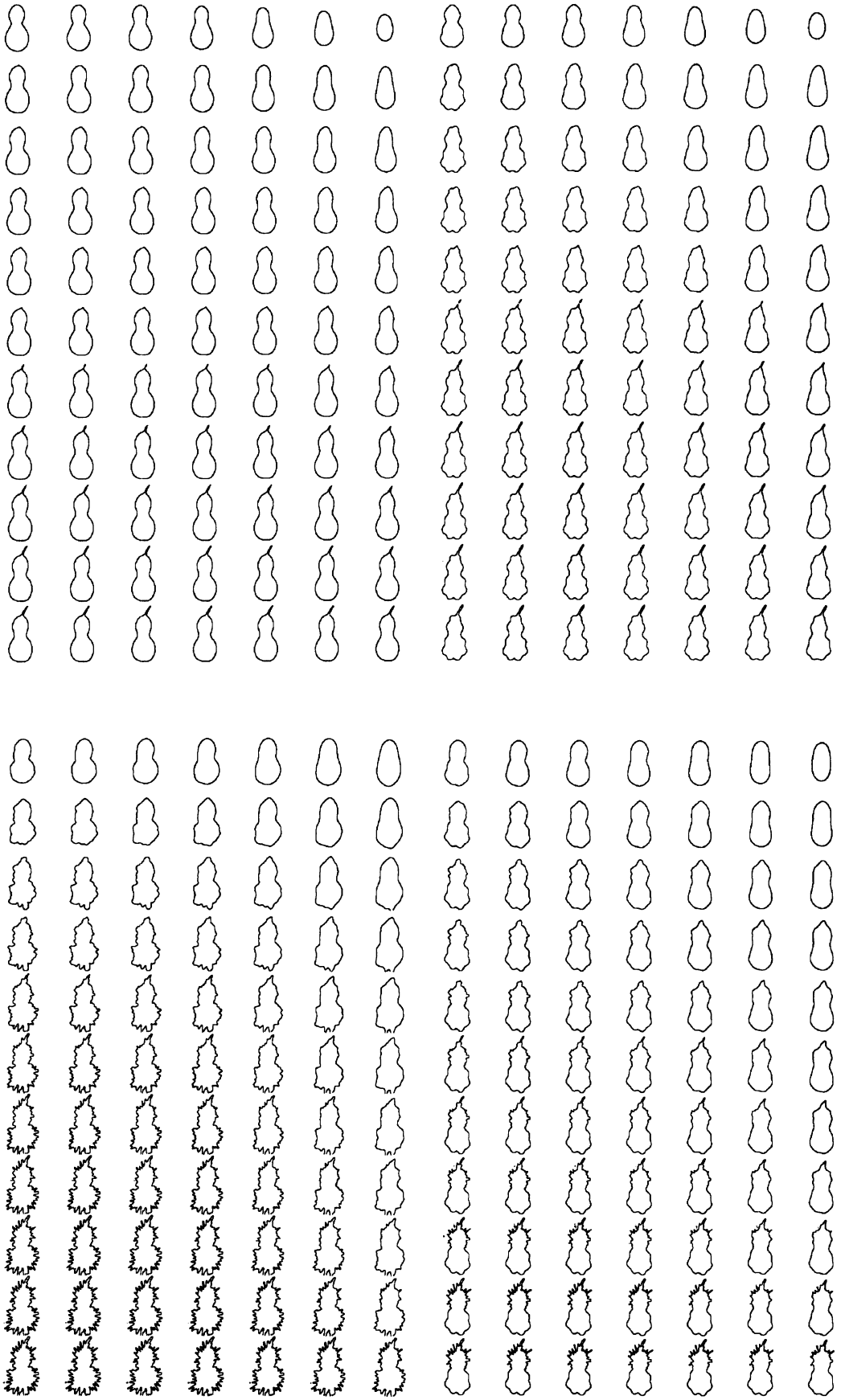

Figure 9: This figure represents the left half portion of Entropy scale-space for the four pears (128x128 binary images). Note that while the right columns depict parabolic diffusion, the left columns depict morphological smoothing. The intermediate columns depict combinations of the these two extremes of smoothing.

References

[1] L. Alvarez, P.-L. Lions, and J.-M. Morel. Image selective smoothing and edge detection by nonlinear diffusion: II. *SIAM Journal of Numerical Analysis*, 29(3):845–866, June 1992.

[2] S. B. Angenent. The zero set of a solution of a parabolic equation. *J. für die Reine und Angewandte Mathematik*, 390:79–96, 1988.

[3] S. B. Angenent. Parabolic equations for curves on surfaces, I. Technical Report Technical Summary reports, 89-19, University of Wisconsin, 1989.

[4] S. B. Angenent. Parabolic equations for curves on surfaces, II. Technical Report Technical Summary reports, 89-24, University of Wisconsin, 1989.

[5] A. Arehart, L. Vincent, and B. B. Kimia. Mathematical morphology: The Hamilton-Jacobi connection. In *Fourth International Conference on Computer Vision (Germany, Berlin, May 11–13, 1993)*, Washington, DC, 1993. Computer Society Press.

[6] J. Babaud, A. P. Witkin, M. Baudin, and R. O. Duda. Uniqueness of the gaussian kernel for scale-space filtering. *IEEE Trans. Pattern Analysis and Machine Intelligence*, 8(1):26–33, January 1986.

[7] P. J. Burt and E. H. Adelson. The laplacian pyramid as a compact image code. *IEEE Transactions on Communications*, 31(4):532–540, April 1983.

[8] F. W. Campbell and J. G. Robson. Applications of fourier analysis to the visibility of gratings. *J. Physiol.(London)*, 197:551–556, 1968.

[9] F. Catté, P.-L. Lions, J.-M. Morel, and T. Coll. Image selective smoothing and edge detection by nonlinear diffusion. *SIAM Journal of Numerical Analysis*, 29(1):182–193, February 1992.

[10] M.-H. Chen and P.-F. Yan. A multiscale approach based on morphological filtering. *IEEE Trans. Pattern Analysis and Machine Intelligence*, 11(7):694–700, July 1989.

[11] M. G. Crandall and P.-L. Lions. Viscosity solutions of Hamilton-Jacobi equations. *Trans. Amer. Math. Soc.*, 277:1–42, 1983.

[12] P. Garabedian. *Partial Differential Equations.* John Wiley and Sons, 1964.

[13] M. A. Grayson. The heat equation shrinks embedded plane curves to round points. *J. Differential Geometry*, 26:285–314, 1987.

[14] M. A. Grayson. Shortening embedded curves. *Annals of Mathematics*, 129:71–111, 1989.

[15] R. M. Haralick, S. R. Sternberg, and X. Zhuang. Image analysis using mathematical morphology. *IEEE Trans. Pattern Analysis and Machine Intelligence*, 9(4):532–550, July 1987.

[16] E. Hopf. The partial differential equation $u_t + uu_x = \epsilon u_x x$. *Comm. Pure Appl. Math.*, 3:201–230, 1950.

[17] R. Hummel, B. B. Kimia, and S. W. Zucker. Deblurring gaussian blur. *Computer Vision, Graphics, and Image Processing*, 38:66–80, 1987.

[18] B. B. Kimia. Conservation laws and a theory of shape. Ph.D. dissertation, McGill Centre for Intelligent Machines, McGill University, Montreal, Canada, 1990.

[19] B. B. Kimia, A. R. Tannenbaum, and S. W. Zucker. Toward a computational theory of shape: An overview. CIM-89-13, McGill Centre for Intelligent Machines, McGill University, Montreal, Canada, 1989.

[20] B. B. Kimia, A. R. Tannenbaum, and S. W. Zucker. Toward a computational theory of shape: An overview. In O. Faugeras, editor, *Lecture Notes in Computer Sceience, 427*, pages 402–407, Berlin, 1990. Springer Verlag.

[21] B. B. Kimia, A. R. Tannenbaum, and S. W. Zucker. Entropy scale-space. In C. Arcelli, editor, *Visual Form: Analysis and Recognition*, pages 333–344, New York, May 1991. Plenum Press.

[22] B. B. Kimia, A. R. Tannenbaum, and S. W. Zucker. On the evolution of curves via a function of curvature, I: The classical case. *JMAA*, 163(2), January 1992.

[23] B. B. Kimia, A. R. Tannenbaum, and S. W. Zucker. Shapes, shocks, and deformations, I: The components of shape and the reaction-diffusion space. *International Journal of Computer Vision*, Submitted, 1992.

[24] B. B. Kimia, A. R. Tannenbaum, and S. W. Zucker. On the role of generalized function theory in computer vision. *In Preparation*, 1993.

[25] J. J. Koenderink. The structure of images. *Biological Cybernetics*, 50:363–370, 1984.

[26] J. J. Koenderink and A. J. van Dooran. Visual detection of spatial contrast: Influence of location in the visual field, target extent and illuminance level. *Biological Cybernetics*, 30:157–167, 1978.

[27] J. J. Koenderink and A. J. van Doorn. Dynamic shape. *Biolological Cybernetics*, 53:383–396, 1986.

[28] P. D. Lax. *Shock Waves and Entropy*, pages 603–634. Academic Press, New York, 1971.

[29] P. D. Lax. *Hyperbolic Systems of Conservation Laws and the Mathematical Theory of Shock Waves.* SIAM Regional Conference series in Applied Mathematics, Philadelphia, 1973.

[30] P. D. Lax. Shock waves, increase of entropy and loss of information. Technical Report DOE/ER/03077-240, Courant Mathematics and Computing Library- R&D Report, 1984.
[31] F. Leymarie and M. D. Levine. Shape features using curvature morphology. In *Proceedings of the SPIE "Intelligent Robots and Computer Vision VIII: Algorithms and Techniques" Conference*, volume 1192, part 2, pages 536–547, Philadelphia, Penn., USA, November 1989.
[32] P. Maragos. Pattern spectrum and multiscale shape representation. *IEEE Trans. Pattern Analysis and Machine Intelligence*, 11(7):701–716, July 1989.
[33] D. Marr and E. Hildreth. Theory of edge detection. Technical Report MIT AI Memo 518, MIT AI Lab, 1979.
[34] H. Matano. Non-increase of the lapnumber of a solution for a one dimensional semilinear parabolic equation. *J. Fac. Sci. Univ. Tokyo IA Math.*, 29:401–441, 1982.
[35] F. Mokhtarian and A. Mackworth. Scale-based description of planar curves and two-dimensional shapes. *PAMI*, 8:34–43, 1986.
[36] O. Oleinik. Discontinuous solutions of nonlinear differential equations. *Amer. Math. Soc. Transl. Ser. 2*, 26:95–172, 1957.
[37] P. Perona and J. Malik. Scale-space and edge detection using anistropic diffusion. *IEEE Trans. Pattern Analysis and Machine Intelligence*, 12(7):629–639, July 1990.
[38] W. Richards, B. Dawson, and D. Whittington. Encoding contour shape by curvature extrema. *Journal of Optical Society of America*, 3(9):1483–1489, 1986.
[39] A. Rosenfeld and M. Thurston. Edge and curve detection for visual scene analysis. *IEEE Trans. Comput.*, C-20:562–569, 1971.
[40] G. Sapiro and A. Tannenbaum. Affine invariant scale-space. *International Journal of Computer Vision*, To Appear, 1993.
[41] G. Sapiro and A. Tannenbaum. On affine plane curve evolution. *Journal of Functional Analysis*, To Appear, 1993.
[42] G. Sapiro and A. Tannenbaum. On invariant curve evolution and image analysis. *Indiana Univ. Journal of Mathematics*, To Appear, 1993.
[43] J. Serra, editor. *Image Analysis and Mathematical Morpholpogy.* Academic Press, 1982.
[44] J. Serra, editor. *Image Analysis and Mathematical Morpholpogy, Part II: Theoretical Advances.* Academic Press, 1988.
[45] J. Smoller. *Shock Waves and Reaction-Diffusion Equations.* Springer-Verlag, New York, 1983.
[46] D. Widder. *The Heat Equation.* Academic Press, 1975.
[47] H. R. Wilson and J. R. Bergen. A four mechanism model for threshold spatial vision. *Vision Research*, 19(1):19–32, 1979.
[48] A. P. Witkin. Scale-space filtering. In *Proceedings of the* 8^{th} *International Joint Conference on Artificial Intelligence*, pages 1019–1022, Karlsruhe, West Germany, August 1983.
[49] A. L. Yuille and T. A. Poggio. Scaling theorems for zero crossings. *IEEE Trans. Pattern Analysis and Machine Intelligence*, 8(1):15–25, January 1986.
[50] S. W. Zucker and R. Hummel. Receptive fields and the representation of visual information. *Human Neurobiology*, 5:121–128, 1986.